Journal of Research in Health Sciences
ISSN: 2228-7809 | https://jrhsjournal.com

Laser Interference Patterning during MBE Growth: Implications for Biocompatible Surface Design in Medical Devices

Dr. L. Chen[1], Dr. J. Walker[1]*, Dr. K. Park[1], Dr. H. Zhao[1,2]

[1] Department of Clinical Engineering and Medical Systems, University of Glasgow, Glasgow G12 8QQ, United Kingdom
[2] School of Public Health and Biomedical Sciences, Shanghai Jiao Tong University School of Medicine, Shanghai 200025, China

ABSTRACT

Single-pulse laser interference is applied to a Molecular Beam Epitaxy growth chamber to achieve in-situ patterning during the growth of III-V materials, with a focus on producing arrays of III-V quantum dots. We will describe the construction and characterization of the interference system as well as the in-situ patterning results. Pulsed laser interference is shown to strongly interact with the growing surface to produce periodic nanoscale features such as holes and islands, the nature of which is dependent on the local surface energy distribution. We describe a mechanism for the formation of these features in terms of surface diffusion under the influence of the periodic thermal gradient induced by the interference pattern. Nanoislands formed at the interference minima are shown to be ideal sites for quantum dot nucleation.

Keywords: Laser interference, nanosecond laser, nanopatterning, nanostructures, nanoholes, nanoislands, quantum dots.

1. INTRODUCTION

Periodic or quasi-periodic nanostructures on the surface of metals, polymers or semiconductors exhibit tremendous potential in optoelectronics [1], nanoelectronics [2], biomaterials [3]. Particularly, ordered arrays of semiconductor nanostructures, e.g. quantum dots (QDs), nanowires (NWs) have attracted increasing attention due to their unique electronic and optical properties for applications from photonic crystals [4] to quantum information processing [5]. Conventional lithographic techniques such as electron beam lithography [6], focused ion beam lithography [7] and atomic-force-microscope (AFM)-based patterning [8] have been widely used to fabricate periodic nanostructures. However, these methods have an inherently high equipment cost and a low processing throughput. In addition, as ex-situ techniques, defects and impurities on the atomic scale are introduced and these limit the performance. In recent years, laser interference lithography has emerged as a fast, cost-effective approach to fabricate large-scale, one-, two- or three-dimensional ordered structures at the nanoscale to achieve advanced device or material performance [9,10]. Such a non-invasive technique can be compatible with epitaxial reactors to achieve in-situ direct patterning on substrates. The application of laser interference to the in-situ structuring of epitaxial growth was first reported by Clegg et al [11], with two beam interference applied to an InGaAs layer grown by MBE. The results showed a 2D modulation of the QD density which they explained by the migration of indium from regions of high temperature at the interference maxima which then condense on the cooler regions of the pattern to form quantum dots. The significance of this work is that it indicates that the near surface absorption of short (few ns) pulses of moderate energy (~50 mJ) is sufficient to raise the surface temperature enough to induce indium surface migration over several hundred nanometers on a very short timescale. However, the limitations of two beam interference and other factors result only in a weak modulation of the quantum dot density rather than specific site location. Subsequently, in-situ four beam interference patterning was realized by Zhang et al [12]. The results show that the patterning of sub-threshold InAs layers results in the formation of nano-islands of various sizes due to variations in the laser intensity over the pattern area. With further indium deposition these islands transform into well-ordered QD arrays. The ordering is precise, but the samples show a large variation in the number of dots per site and a broad distribution of dot sizes. The authors attribute their observations to the removal of indium by desorption in the high intensity regions of the pattern, which is somewhat contrary to the suggestion of indium diffusion induced nucleation of Clegg. In this work, we demonstrate the direct (resist-free) laser interference patterning of Molecular Beam Epitaxy (MBE) growth surfaces

and provide further evidence that the InAs QDs are nucleated around the nanoislands induced by surface diffusion process due to laser interference.

*m.hopkinson@sheffield.ac.uk; phone +44 114 222 5385; nanostencil-eu.com

Surface features such as arrays of nanoholes and islands with a pitch corresponding to the interference pattern (~ 300 nm pitch) are created depending on the laser energy variation across the surface. On to such island features we are able to achieve long-range ordered arrays of InAs quantum dots which are ideal building blocks for future nanoscale circuits.

2. THEORETICAL SIMULATIONS

Multi-beam interference can be considered as a linear superposition of multiple light waves satisfying the wave function. To simplify the theoretical analysis, a Gaussian laser beam can be approximated as a uniform plane wave when both the divergence angle and interference area are small. The total intensity of the interference field of *n* coherent beams can be written as

$$I = \left|\sum_{i=1}^{n} A_i \cdot \vec{P}_i \cdot exp\left[-i\left(\left(\frac{2\pi}{\lambda}\right)\sin\theta_i(cos\varphi_i \cdot x + sin\varphi_i \cdot y) + \delta_i\right)\right]\right|^2 \quad (1)$$

and

$$\vec{P}_i = -(cos\theta_i cos\Psi_i cos\varphi_i - sin\varphi_i sin\Psi_i) \cdot x - (cos\theta_i cos\Psi_i sin\varphi_i + cos\varphi_i sin\Psi_i) \cdot y \quad (2)$$

where A_i is the amplitude, $\overrightarrow{P_i}$ is the unit polarization vector, λ is the wavelength of laser, θ_i represents the angle of incidence, φ_i is the azimuth angle, and Ψ_i is the polarized angle and δ_i is the initial phase. The pitch of the pattern is proportional to the wavelength of laser and inversely proportional to the angle of incidence. In this work, four-beam laser interference using the 3rd harmonic of Nd-YAG at λ=355 nm is described. All the theoretical modelling was performed using MATLAB. The amplitudes of four beams are assumed to be identical and the initial phases are all zero. Four laser beams follow a configuration with the identical incidence angle of θ=58° using azimuth angles of 0°, 90°, 180° and 270°. The intensity distribution patterns are presented in Figure 1, with different polarized angles and different beam intensity ratio. Figure 1(a)-(e) illustrate that the polarization state of beams can change the distribution pattern and also affect the contrast of the pattern, and Figure 1(f) shows the pattern is also strongly influenced by the uneven energy distribution of four beams. A Moiré pattern, namely an amplitude modulation with a macroscopic pitch, can be generated when the incidence angles or azimuth angles are not exactly identical. Figure 1(g)(f) show the interference pattern with amplitude modulation with the incidence angle offset of 1-2° and different energy intensity ratio, where the polarized angles are 58° and the azimuth angles keep unchanged.

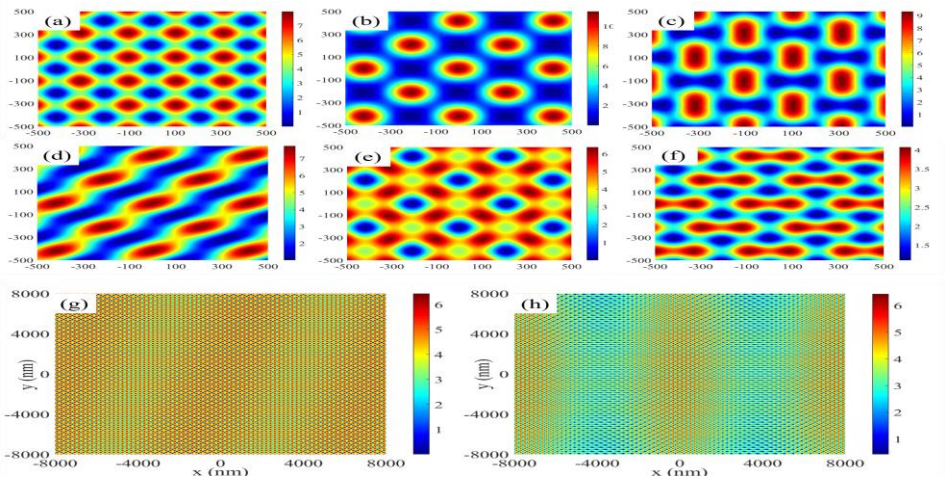

Figure 1. Four-beam interference intensity distribution at the incident angle of 58° but with different polarization angles (a) $\Psi_1 = \Psi_2 = \Psi_3 = \Psi_4 = 90°$, (b) $\Psi_1 = \Psi_2 = \Psi_3 = \Psi_4 = 0°$, (c) $\Psi_1 = \Psi_3 = 90°$, $\Psi_2 = \Psi_4 = 0°$, (d) $\Psi_1 = 90°$, $\Psi_2 = \Psi_3 = \Psi_4 = 0°$, (e) $\Psi_1 = \Psi_2 = \Psi_3 = \Psi_4 = 58°$, (f) beam intensity ratio I_1:I_2:I_3:I_4=0.1:1:0.1:1 at polarized angles of 0°,

3. IN-SITU MBE-LASER PATTERNING CONFIGURATION

In our approach, four-beam laser interference is applied to the MBE substrate surface at an angle of incidence of 58° via four symmetric anti-reflective optical vacuum viewports facing upwards and positioned in the lower half of the MBE system. Laser pulses are applied from a flashlamp pumped Nd:YAG laser (Innolas Spitlight) operating at the wavelength of 355 nm and *P*-polarization, and with a pulse width of 7 ns, a 5 Hz repetition rate and a pulse energy in the range of 10-50 mJ. The beam diameter is around 5 mm. The lithography arrangement is shown in simplified schematic form in Figure 2. The beam is split to produce four symmetric beams which interfere on the substrate surface. PM1 &2 are periscope mirrors which are used to change the height of the beam to the same height of the MBE optical ports. BS1-3 are beam splitters and M1-6 are mirrors. A half wave plate (H) and polarizer (P) is present in each beam to adjust the polarized angles. The laser is positioned on an optical bench adjacent to the MBE system and the beam directed to a set of optics positioned onto the MBE sub-frame. All the optics in Figure 2 are on the MBE system and only a beam steering mirror and an external shutter are on the optical bench (however the bench also contains a prototyping interference arrangement, which is not shown). Photographs of some of the optics on the MBE system are shown in Figure 3.

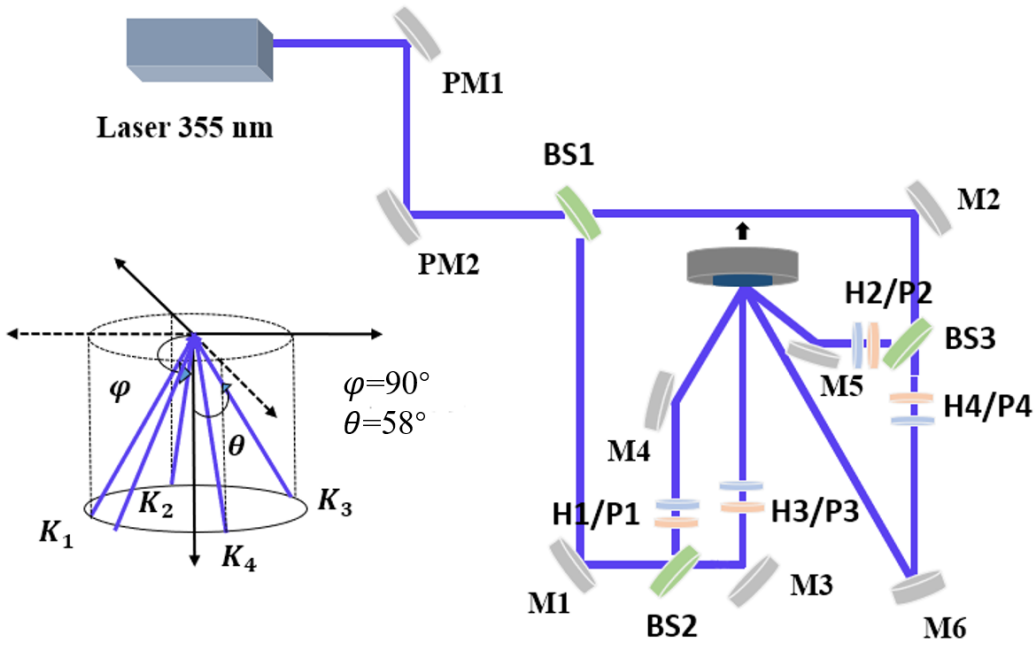

Figure 2. Simplified schematic of laser interference system used for MBE growth patterning.

Beam alignment is performed by means of an upward facing camera in a surface normal viewport. At the substrate position, we use a 2-inch InGaN/GaN wafer to view the UV laser pulses. The InGaN absorbs the UV light and emits blue luminescence which can be imaged by the CMOS camera. The insert in Figure 3 shows the image of 4 beams aligned on the center of the wafer, which is sitting on the MBE substrate stage. One can see an elliptical projection of the beams due to the rather large (58°) incidence which reduces the overlap area intensity and size. We are working on methods to improve this by expanding the beam in the horizontal direction using cylindrical lenses.

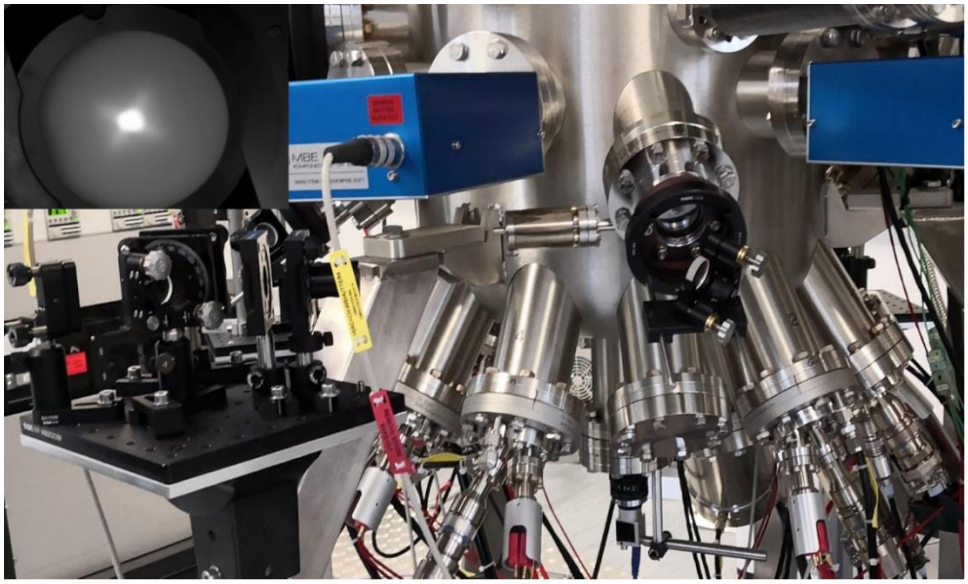

Figure 3. Beam splitter optics and optical viewport with guiding mirror positioned on the MBE system. Inset shows the camera image of 4 beams aligned on the center of the 50 mm InGaN wafer.

4. EXPERIMENTAL RESULTS AND DISCUSSION

The samples were grown on 2-inch GaAs(100) wafers using MBE system on a 500 nm GaAs buffer layer prepared at a substrate temperature of 600°C, after which the substrate was cooled to 500°C at which temperature the pulses were applied. In our first growths, we observed the formation of nanoholes towards the wafer center where the beam overlap is the strongest, as shown in the AFM image in Figure 4(a). In this region we believe the pulse energy to be in the range of 40-50 mJ/cm^2. The nanoholes are ~60-80 nm wide and 2-4 nm deep and are often accompanied by Ga droplets. We believe that in these regions the peak fluence is sufficient to dissociate GaAs, leading to arsenic evaporation and releasing free Ga which then tends to cluster together to form droplets. This implies an instantaneous surface temperature maximum of >650°C. Ga droplets are formed on the colder regions, between the holes, here the surface temperature is lower and at such a temperature Ga can recombine with As and crystallize as GaAs islands.

Figure 4. 5×5μm^2 AFM images of a sample surface with (a) nanoholes and (b) nanoislands patterned by single-pulse laser interference patterning on GaAs substrate grown by MBE.

At lower energies we observe the formation of nanoislands, as shown in Figure 4(b). The island growth is associated with lower energies in the range of 10-30 mJ/cm^2. These shallow islands are 80-120 nm wide and only ~1 nm (2-3 monolayer)

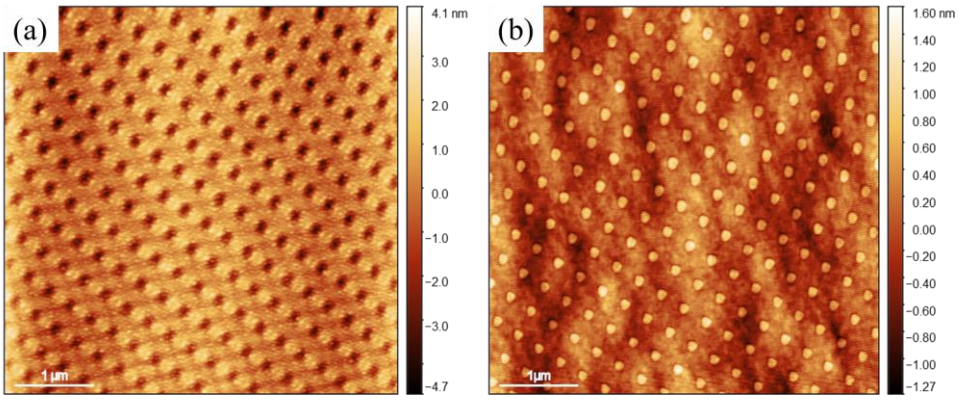

high. The formation of these nanoislands originates from interference-induced surface diffusion at the nanoscale, which is due to thermal gradients generated by the interference intensity distribution. The laser pulses are applied to GaAs surfaces

during MBE growth and strongly absorbed at the surface resulting in transient thermal gradients, so that the adatoms move from interference maxima regions to interference minima regions [13]. In fact, we observe nanoholes and nanoislands in the same sample due to a laser intensity variation over overlap pattern. These two surface features represent the two extremes of a wide range of patterns that we see, which include 'hole-like' and 'island' like features. The reason why we see a wide variation in patterns in a single experiment can come from a number of possible origins. From our observations, it is clear that there are varying proportions of the 4 beams at different region of the wafer. These may be due to beam misalignment, beam profile or pointing stability issues. In this case one or more of the beams can become significantly weaker. There is also a well-known Moiré effect, which can be due to slight misalignment of the azimuthal or incidence angle which we have seen in the simulation results shown in Figure 1(g-h). This typically produces a further periodic intensity modulation, when the angle offset is small, the pitch will be larger ~100-300 um.

For the following samples, 1.6 ML of InAs was deposited with a growth rate of 0.079 ML s^{-1} on the GaAs buffer layer. During this growth process, single-pulse laser interference patterning was employed just after 1 ML of InAs deposition, which is below the critical thickness, after which additional 0.6 ML InAs was supplied. For the growth on such a nanoisland-structured surface, it is expected that the nucleation of QDs to be mainly determined by the surface morphology.

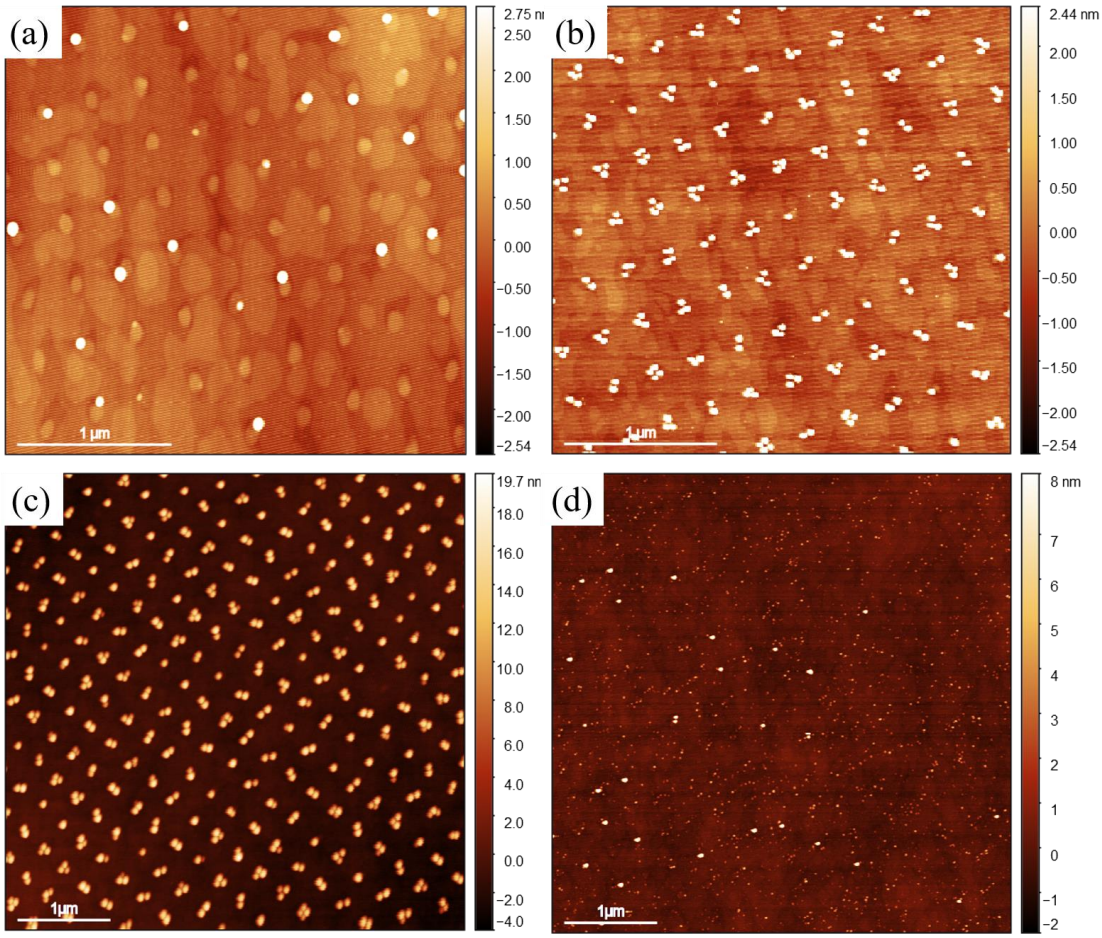

Figure 5. 3×3µm^2 AFM images of a sample surface with InAs QD nucleation at the edge of (a) big nanoislands and (b) small nanoislands. (c) A 5×5µm^2 AFM images of typical QD arrays with a pitch of 300 nm formed by 4-beam interference patterning. (d) Non-patterned region (wafer edge) with bimodal size distribution of QDs.

This is indeed what we observe and nucleation of QDs at the edge of the nanoislands has been found reliability in more than 20 samples. Figure 5(a) demonstrates that InAs QDs are preferably nucleated at the edge of nanoislands and that more QDs are formed at relatively smaller islands (Figure 5(b)). The results suggest that indium diffusion is strongly promoted

to reach the critical thickness at the interference minima whilst being largely suppressed on the planar areas between the pattern sites. With decreased island size, more indium atoms can accumulate within the concentrated area, giving rise to a high nucleation rate for QDs. Figure 5(c) shows a typical AFM image of a patterned QD region. The QDs have excellent site positioning on an array of around 300 nm pitch, with a width of 40-50 nm and height of 12-15 nm. Compared to this region, the non-patterned region shown in Figure 5(d) has small QDs which are randomly nucleated and have a bimodal size distribution with a density of 1×10^{10} cm^{-2}, indicating that the InAs coverage is below the optimal value for a homogeneous distribution. The patterned region exhibits a much lower QD density (~2×10^{9} cm^{-2}) with enlarged dots and better size uniformity.

We believe that our results are consistent with a model of indium surface diffusion under the influence of a transient thermal gradients, as previously suggested by our thermal calculations [13]. The results are consistent with the methodology proposed by Clegg [11] and imply that nanostructuring occurs due to adatom surface diffusion to the colder regions of the pattern (interference minima). This process must be extremely fast as it has to occur over the very short (<μs) timescales at which the surface temperature is raised by laser absorption. Unlike the explanation of Zhang [12], we see no clear evidence for indium desorption. In fact, in our previous calculations [13] we suggested that indium desorption would be insignificant because of the relatively short timescale of the transient. In our studies, we establish, for the first time, that the formation of nanoscale islands is the precursor for QD formation and that QD nucleation only occurs for the smallest of these islands (<100 nm) in which the local indium content is the most concentrated. In the work of Zhang there is no correlation between the QD patterning and the underlying morphology and it would seem difficult to explain the island formation solely through desorption of large regions of the surface. In addition, we observed that the QDs can be formed in the patterned region even at low InAs coverage below the critical thickness, which implies the net indium content is not reduced in the patterned region as would be the case with desorption. The process must be a local enhancement rather than a local loss of indium. Like Clegg, we see strong justification for a diffusion-based mechanism with a well-defined temperature threshold and with rapid diffusion over the short timescale of the laser transient which creates a patterned morphology which can act as a nucleation site for QDs and perhaps for other nanostructures.

5. CONCLUSION

In conclusion, we describe the application of pulsed laser interference to Molecular Beam Epitaxy growth. The technique combines the simplicity of in situ laser interference patterning with self-assembly to achieve ordered nanostructures, such as quantum dots for which we describe the growth of InAs on GaAs substrates. Single pulse interference on the MBE growth surface is observed to be capable of manipulating the surface atomic kinetics to promote nanohole or nanoisland formation, as well as a wealth of other pattern features. Periodic arrays of nanoislands yield energetically favourable nucleation sites for QDs which nucleate at the edge of islands. Excellent lateral ordering of single QDs or QD molecules has been obtained, guided by the presence of nanoislands. Although our results are specific to III-V MBE, the technique can be applicable to other materials and growth technologies which have thermally activated growth processes. This novel technique provides a fast and efficient means for providing highly ordered arrays of nanostructures and offers a template for the realization of novel devices relying on single QDs or QD molecules.

ACKNOWLEDGMENT

The authors gratefully acknowledge support from the EU H2020 program ‘Nanostencil’ and EPSRC.

REFERENCES

[1] Leung, S., Zhang, Q., Xiu, F., Yu, D., Ho, J., Li, D. and Fan, Z., "Light Management with Nanostructures for Optoelectronic Devices," The Journal of Physical Chemistry Letters, 5(8), 1479-1495 (2014).
[2] Osada, M. and Sasaki, T., "Two-Dimensional Dielectric Nanosheets: Novel Nanoelectronics From Nanocrystal Building Blocks, " Advanced Materials, 24(2), 210-228 (2011).
[3] Luo, Q., Hou, C., Bai, Y., Wang, R. and Liu, J., "Protein Assembly: Versatile Approaches to Construct Highly Ordered Nanostructures," Chemical Reviews, 116(22), 13571-13632 (2016).

[4] Rigal, B., Dwir, B., Rudra, A., Kulkova, I., Lyasota, A. and Kapon, E., "Single photon extraction and propagation in photonic crystal waveguides incorporating site-controlled quantum dots," Applied Physics Letters, 112(5), 051105 (2018).
[5] O'Brien, J., Furusawa, A. and Vučković, J., "Photonic quantum technologies," Nature Photonics, 3(12), 687-695 (2009).
[6] Jons, K. D., Atkinson, P., Muller, M., Heldmaier, M., Ulrich, S. M., Schmidt, O.G., and Michler, P., "Triggered indistinguishable single photons with narrow line widths from site-controlled quantum dots," Nano Lett., 13(1), 126-130 (2012).
[7] Lee, J., Saucer, T. W., Martin, A. J., Tien, D., Millunchick, J. M., and Sih, V., "Photoluminescence imaging of focused ion beam induced individual quantum dots," Nano Lett.,11(3), 1040-1043 (2011).
[8] Kim, Y., Na, K., Choi, S. and Yang, S., "Atomic force microscopy-based nano-lithography for nano-patterning: a molecular dynamic study," Journal of Materials Processing Technology, 155-156, 1847-1854 (2004).
[9] Domínguez, S., García, O., Ezquer, M., Rodríguez, M., Lagunas, A., Pérez-Conde, J. and Bravo, J., "Optimization of 1D photonic crystals to minimize the reflectance of silicon solar cells," Photonics and Nanostructures - Fundamentals and Applications, 10(1), 46-53 (2012).
[10] Dyck, T., and Haas, S., "A model for direct laser interference patterning of ZnO:Al - predicting possible sample topographies to optimize light trapping in thin-film silicon solar cells," Applied Physics A, 122(4) (2016).
[11] Clegg, C., and Yang, H., "Guided assembly of quantum dots through selective laser heating," Solar Energy Materials and Solar Cells, 108, 252-255 (2013).
[12] Zhang, W., Shi, Z., Huo, D., Guo, X., Zhang, F., Chen, L., Wang, Q., Zhang, B. and Peng, C., "In-situ laser nano-patterning for ordered InAs/GaAs(001) quantum dot growth," Applied Physics Letters, 112(15), 153108 (2018).
[13] Wang, Y. R., Jin, C. Y., Ho, C., Chen, S., Francis, H., Hopkinson, M., "Thermodynamic processes on a semiconductor surface during in-situ multi-beam laser interference patterning," IET Opt., 13(1), 7-11 (2019).